Int. J. Electrochem. Sci., 15 **(2020)** 505 – 514, doi: 10.20964/2020.01.75

International Journal of
ELECTROCHEMICAL
SCIENCE
www.electrochemsci.org

Acetylcholinesterase based rGO-TEPA-Copper nanowires biosensor for detecting malathion

Sheng Li[1,*], *Li Mei Qu*[1], *Jia Fu Wang*[1], *Xue Qin Ran*[2], *Xi Niu*[1]

[1] The Key Laboratory of Plant Resources Conservation and Germplasm Innovation in Mountainous Region (Ministry of Education)/Guizhou Key Lab of Agro-Bioengineering, Institute of Agro-Bioengineering and College of Life Sciences, Guizhou University, Guiyang 550025, Guizhou, China
[2] Faculty of Animal Science and Veterinary Medicine, Guizhou University, Guiyang, China.
[*]E-mail: listen318@163.com

Received: 8 September 2019 / *Accepted:* 3 November 2019 / *Published:* 30 November 2019

This study aimed to develop a biosensor for rapid detection of malathion. We established a biosensor by immobilizing acetylcholinesterase (AChE) to glassy carbon electrode (GCE) with the modification of reduced graphene oxide-tetraethylenepentamine (rGO-TEPA) and the copper nanowires (Cu NWs). The rGO-TEPA-Cu NWs was used to improve the electrode conductivity and enhance the electrode loading ability for AChE. Chitosan (CS) was used to as the supporter for AChE. Exposure to malathion inhibited AChE activity and decreased the current significantly. We optimized the detection condition and found that AChE-CS/rGO-TEPA-Cu NWs/GCE showed a linear association with malathion from 1 ng/mL to 20 μg/mL (R^2=0.989) and the detection limit was 0.39 ng/mL. Furthermore, analysis of real samples using the biosensor showed satisfactory results. In conclusion, the biosensor we developed in this study has potential application to the detection of organophosphate insecticides such as malathion.

Keywords: malathion; organophosphate insecticides; biosensor; nanowire; acetylcholinesterase

1. INTRODUCTION

Organophosphate (OP) insecticides are widely used in agricultural production, and cause a series of problems on human health, food safety and environment because of its toxicity and bioaccumulation effect [1]. Several methods for monitoring organophosphate have been used, such as gas chromatography [2], liquid chromatography [3], fluorimetry [4] and ultraviolet spectroscopy [5]. Although these methods have a good accuracy, they have some shortcomings such as time-consuming, complicated sample pretreatment steps and high standards for professional technicians. Binding enzymes onto electrodes as electrochemical biosensors have attracted more attention because of their simplicity in operation and rapid response [6, 7]. It was reported that acetylcholinesterase (AChE) modified onto the electrode

catalyzed acetylthiocholine chloride (ATCl) hydrolysis and showed irreversible peak of current [8]. The exposure to OPs could inhibit AChE activity and decrease the current [9].

Recently, nanomaterial/nanocomposites have been used to fabricate AChE biosensor with improved conductivity, stability and sensitivity [10-12]. In particular, graphene exhibits exceptional properties, including high conductivity, satisfactory mechanical strength, and excellent bio-compatibility [13-15].

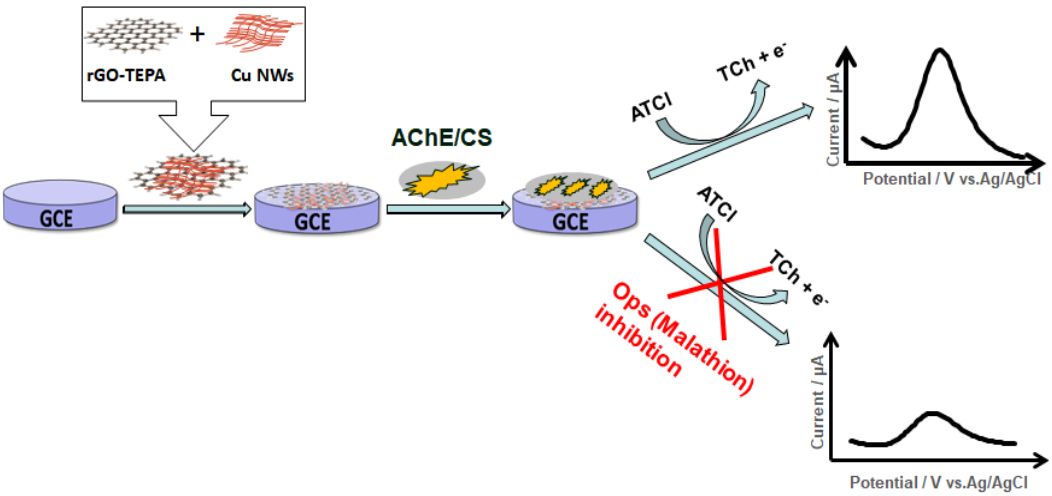

Scheme 1. Fabrication of AChE-Cs/rGO-TEPA-Cu NWs/GCE biosensor.

In this study, we developed AChE biosensor for quantitative detection of the malathion, which is a typical organophosphate insecticide. The AChE biosensor was modified by reductive graphene oxide-tetraethylenepentamine (rGO-TEPA) and Cu nanowires (Scheme 1). rGO-TEPA is a novel nanomaterial with excellent conductivity due to covalent modification of rGO and TEPA [16]. Cu is widely used in batteries, solar cells, physical sensors and electrochemical biosensors due to its excellent catalytic and electrochemical properties [17]. CuO nanowires and Pd-Cu nanowires have been utilized for electrochemical detection of organophosphorus [18, 19]. The nanocomposites of rGO-TEPA and Cu NWs can form a dense network structure, which significantly improves the specific surface of the sensor and enhances the detection sensitivity. To our knowledge, this is the first report on the development of AChE sensor based on rGO-TEPA-Cu NWs. In addition, we used chitosan (CS) as a film to support AChE due to excellent bio-compatibility and adsorption [20]. Under a series of optimized conditions, the biosensor showed good performance in detecting malathion.

2. EXPERIMENTAL

2.1 Reagents

AChE (E.C.3.1.1.7, 200 U/mg from electric eel), ATCl (≥99% purity), Malathion (≥99.9% purity) standard substance were purchased from Sigma-Aldrich. rGO-TEPA was from XFNANO Nanotech (Nanjing, China). Potassium ferricyanide $K_3Fe(CN)_6$ and potassium ferrocyanide $K_4Fe(CN)_6$

were from Chemical Reagents (Beijing, China). Copper nitrate $Cu(NO_3)_2$, Hydrazine N_2H_4 and ethylenediamine (EDA) were from ACROS. Chitosan (Cs) was from Sinopharm Chemical Reagent. All other reagents were analytical pure.

2.2 Preparation of Cu NWs

Cu NWs were synthesized according to the method described previously [21]. Briefly, NaOH solution (20 mL) was heated to 60℃, and then $Cu(NO_3)_2$ (0.1 M), EDA and N_2H_4 solution were added successively. The reaction continued at 60℃ for 2 h to obtain a red product (Cu NWs) floating on top of the solution. The Cu NWs was rinsed and dispersed in ethanol for later use.

2.3 Preparation of biosensor

First, glass carbon electrode was carefully polished in alumina slurries, then sonicated to obtain smooth surface. Then 6 μL mixture containing 2mg/mL rGO-TEPA and 1 mg/mL Cu NWs (v/v=2:1) was dropped on electrode, dried in the air at room temperature. Finally, AChE and chitosan were mixed at ratio of 1:10 (w/w) and immobilized on the electrode for 8 h at 4℃.

2.4 Electrochemical analysis

The electrodes were scanned by cyclic voltammetry (CV) (Range -0.2 to +0.6 V, scan rate 100 mV/s) and electrochemical impedance spectroscopy (EIS) (scan rate 10^{-1}-10^5 hz) in 0.1 M KCl solution with 5 mM $[Fe(CN)_6]^{3-/4-}$. The prepared AChE-CS/rGO-TEPA Cu NMs/GCE biosensor was incubated with 2 mM ATCl in phosphate buffered saline (PBS) (0.1 M pH 7.4), and Differential pulse voltammetry (DPV) technique was used to detect the current response. Next, the electrode was rinsed by PBS and transferred into ATCl solution to test the DPV signal after incubation with malathion. The inhibition of malathion was calculated as Inhibition (%) $=\Delta I / I_0 \times 100\%$, $\Delta I = I_0 - I_i$, I_0 and I_i indicated peak current before and after the incubation with malathion, respectively.

2.5 Detection of vegetable samples

Cabbages and carrots were collected from local market, thoroughly washed with water to remove large particles, and mixed with acetone and PBS. The mixture was sonicated for 30 min and centrifuged at 8,000 rpm for 5 min, the supernatants were filtered through 0.45 μM membranes. Then the AChE-CS/rGO-TEPA Cu NMs/GCE electrode was dipped into the supernatants and the inhibition rate was detected.

3. RESULTS AND DISCUSSION

3.1 Identification of nanomaterials

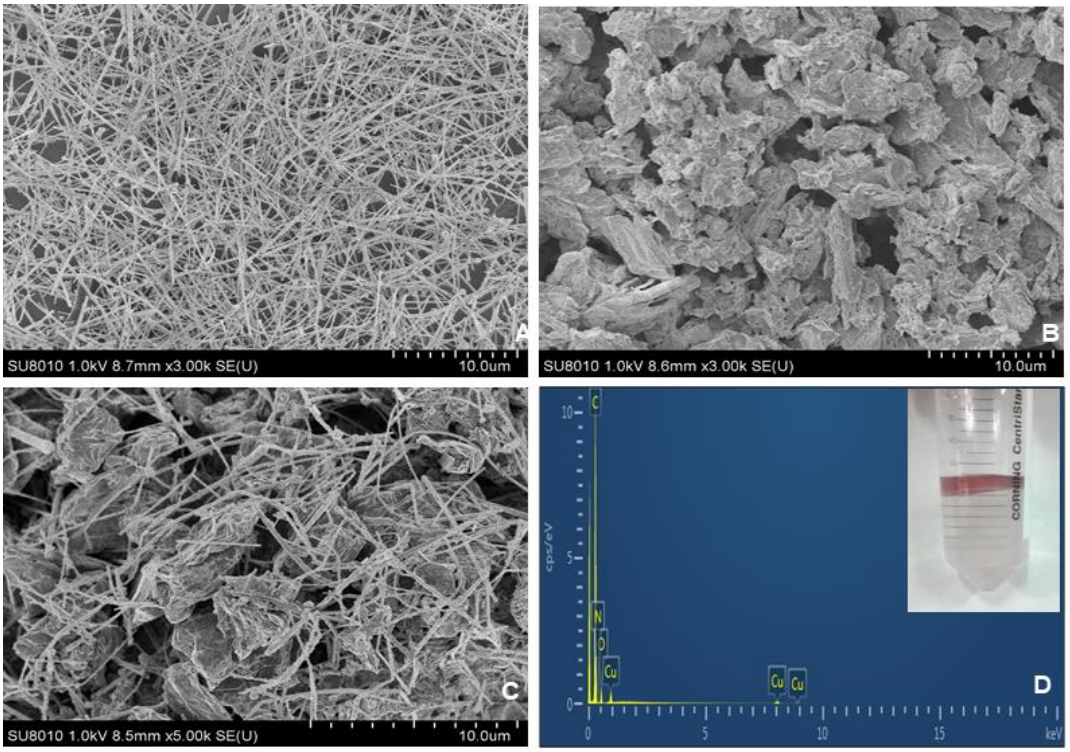

Figure 1. SEM images of Cu NWs and rGO-TEPA (A) Cu NWs, (B) rGO-TEPA, (C) rGO-TEPA-Cu NWs, (D) The EDX image of rGO-TEPA-Cu NWs. The inset showed the photograph of AChE-CS/rGO-TEPA-Cu NWs/GCE, which was red in the tube.

Scan electron microscopy (SEM) was usually applied to determine the morphology of the nanomaterials [22]. As shown in Fig.1A, the SEM image of Cu NWs displayed smooth surface and uniform linear morphology. The Cu NWs was about 10μm long with the diameter were around 80-150nm. The SEM image of rGO-TEPA showed a wrinkled paper-like structure, which provided enough surface area for immobilization enzyme and favored electron transport (Fig.1B) [23]. After rGO-TEPA and Cu nanowires were thoroughly mixed, the slender copper nanowires wrapped around the edge of rGO-TEPA and formed a dense network structure (Fig.1C). Furthermore, the morphology of copper nanowires and rGO-TEPA did not change. To further monitor the formation of rGO-TEPA-Cu NWs, the energy diffraction optical spectroscopy (EDS) was employed to analyze the elements in Cu NWs-rGO-TEPA composite. As shown in Fig.1D, several unique and intense peaks were observed, representing Cu, C, O, and N, respectively. These results suggest that the nanomaterials were successfully synthesized and could be used to immobilize AChE enzyme.

3.2 Electrochemical characterization of the electrode

All electrodes exhibited stable and distinct redox peaks for the redox reaction cycle in $[Fe(CN)_6]^{3-/4-}$ (Fig.2A). The classical reversible redox peaks were first observed on the bare electrode GCE

(curve a). The current response of the electrodes modified with rGO-TEPA-Cu NWs (curve b) increased sequentially, which may be attributed to excellent conductivity and ability to transfer electrons quickly. After the AChE molecules was immobilized on the sensor, the peak current decreased sharply (curve c), because AChE blocked electron transfer between electrode materials [24].

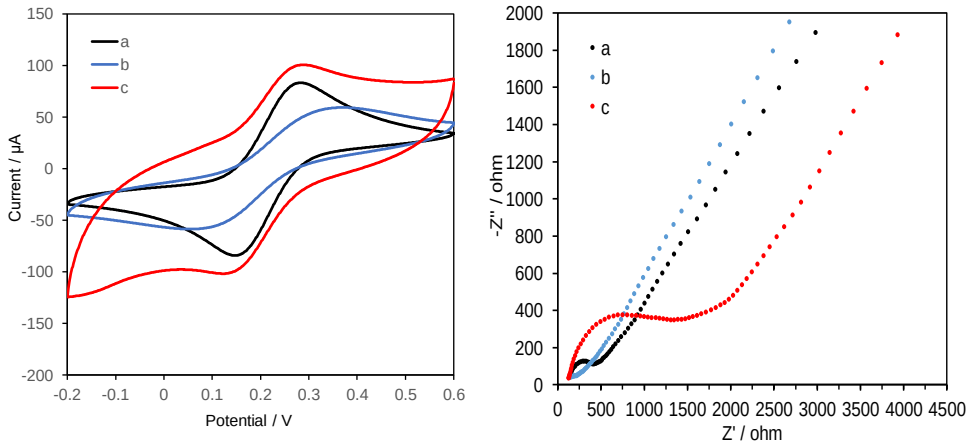

Figure 2. A. The CVs of electrodes. (a) bare GCE, (b) rGO-TEPA-Cu NWs/GCE, (c) AChE-CS/rGO-TEPA-Cu NWs/GCE. Scan rate: 100 mV/s. **B.** The EIS of electrodes. (a) bare GCE, (b) rGO-TEPA-Cu NWs/GCE, (c) AChE-CS/rGO-TEPA-Cu NWs/GCE.

Electrochemical impedance spectroscopy (EIS) is usually used to analyze interfacial properties of electrodes [25]. Fig.2B showed the Nyquist diagram of the electrodes from EIS in $[Fe(CN)_6]^{3-/4-}$ solution. The bare electrode showed a semicircle at the beginning of the curve (curve a). After rGO-TEPA-Cu NWs modification, the semicircle of the curve almost disappeared (curve b). The results indicated that rGO-TEPA-Cu NWs accelerated electron transfer and decreased electrode impedance. When AChE was applied to rGO-TEPA-Cu NWs, the diameter of the semicircle increased significantly (curve c), indicating that acetylcholinesterase was immobilized onto the electrode and increased electrode impedance.

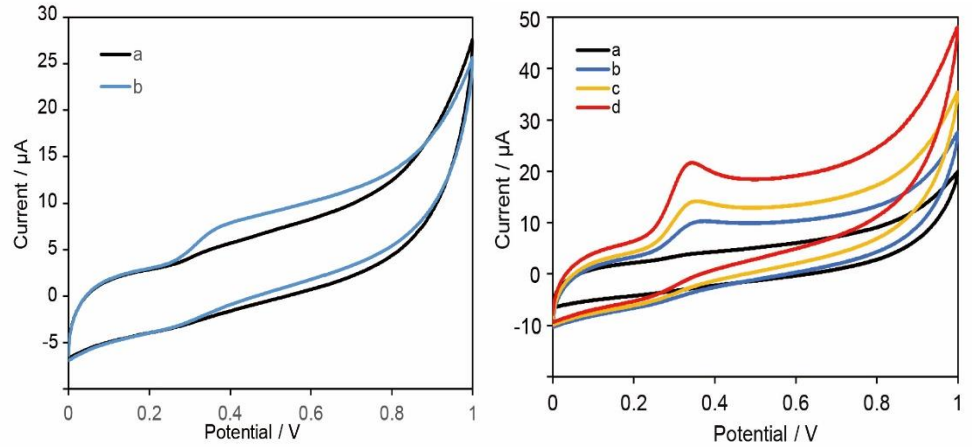

Figure 3. A. CVs of AChE-CS/GCE in blank (a) and 1 mM ATCl (b); **B.** CVs of AChE-CS/rGO-TEPA-Cu NWs/GCE in different concentrations of ATCl, (a) 0 mM, (b) 0.5 mM, (c) 1 mM, (d) 2 mM.

The electrochemical behaviors of the sensor toward ATCl were also examined by CV. AChE-CS/GCE showed a peak in 1 mM ATCl (Fig. 3A, curve b), due to the oxidation of thiocholine (TCh), which was the product of ATCl catalyzed by AChE [26]. Moreover, the peak current of AChE-CS/rGO-TEPA-Cu NWs/GCE at 0.3V increased with the increasing concentrations of ATCl. The peak reached the maximum at 2 mM ATCl. The maximum current (Fig. 3B, curve d) was much higher than peak A (Fig. 3A, curve b), indicating that these materials enhance the sensor electrochemical performance.

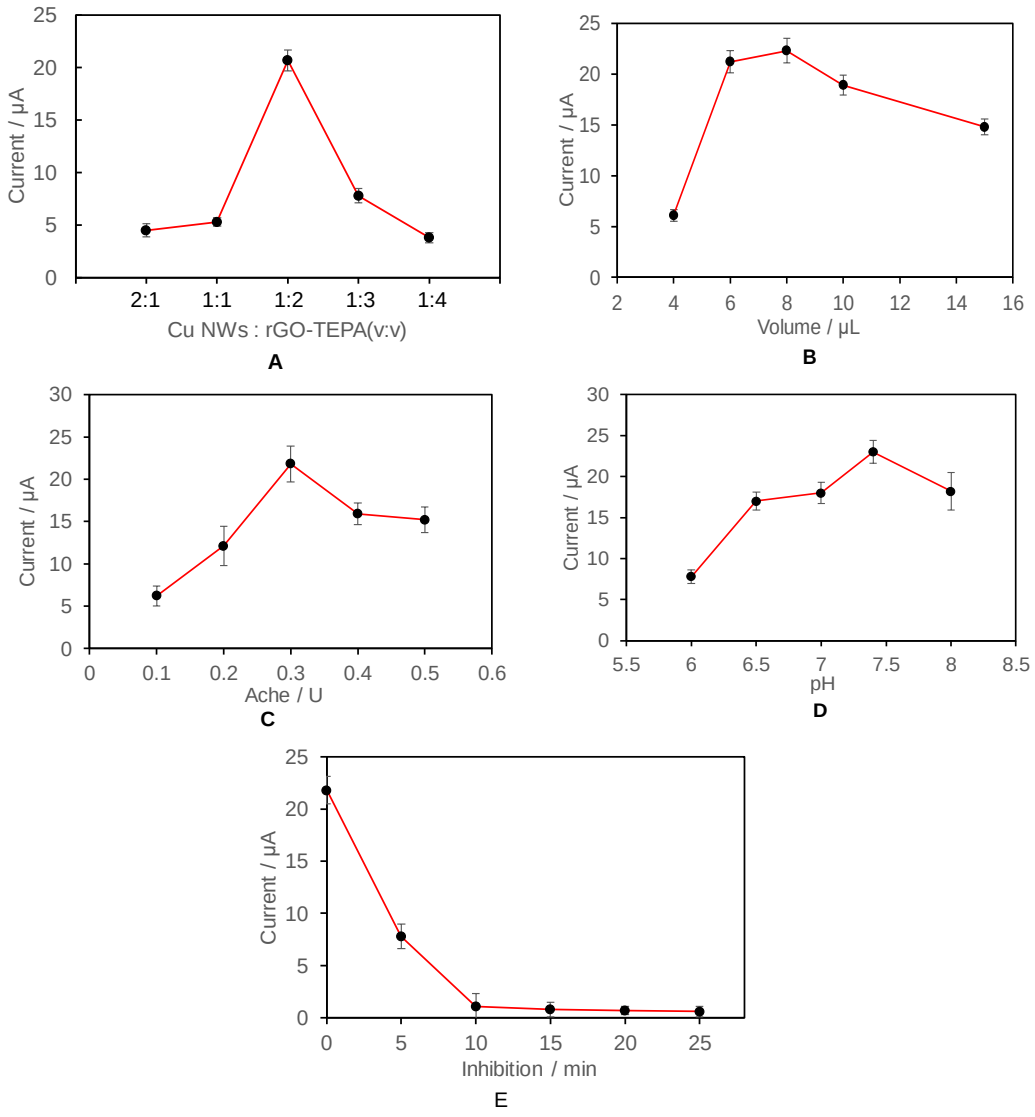

Figure 4. Optimum experiments of AChE-Cs/rGO-TEPA-Cu NWs/GCE sensor by DPV in 1 ng/mL malathion. (A) The ration of Cu NWs and rGO-TEPA, (B) The volume of rGO-TEPA-Cu NWs, (C) The volume of AchE, (D) pH of PBS, (E) The inhibition time.

3.3 Optimization of parameters

To improve the performance of the sensors, several parameters were optimized. The current response of DPV reached the maximum if the ratio of Cu NWs to rGO-TEPA was 1:2 (Fig.4A). After

adding 6 µL rGO-TEPA-Cu NWs, the current response from DPV reached the maximum (Fig.4B). The amount of AChE enzyme on sensor also affected the current signal [27]. The maximum current signal appeared if 0.3 U AChE was immobilized on the electrode and excessive enzyme could increase the electrode resistance (Fig.4C). The pH of PBS can determine the performance of the sensor by affecting enzyme activity [28]. The current response began to decrease after pH 7.4 (Fig.4D), and pH 7.4 was chosen as optimum pH. The current response decreased significantly with increasing incubation time during the first 10 min (Fig.4E). After that, the current signal did not change significantly, suggesting that the binding between malathion and the active sites of AChE may reach the saturation. Therefore, the incubation time of the electrode in malathion was selected to be 10 min.

3.4 Malathion determination

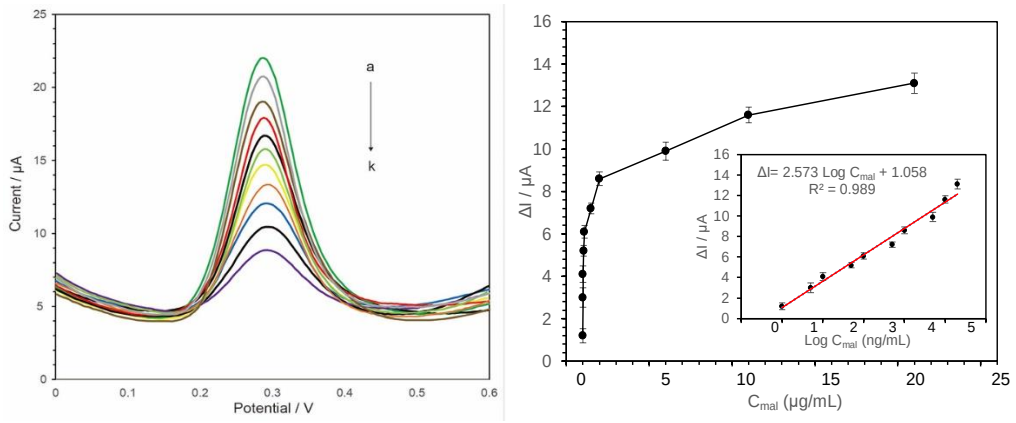

Figure 5. A. DPV responses of AChE biosensor after incubation with different concentrations of malathion for 10 min (a-k): (a) 0 ng/mL (b) 1 ng/mL (c) 5 ng/mL (d) 10 ng/mL (e) 50 ng/mL (f) 100 ng/mL (g) 500 ng/mL (h) 1 µg/mL (i) 5 µg/mL (j) 10 µg/mL (k) 20 µg/mL. B. The corresponding plot of the difference in ΔI against the concentration of malathion. Insets: linear curve of ΔI with the concentration of malathion.

Table 1. The detection range and limit with malathion from different biosensors

Biosensors	Linear range	Detection limit	References
AChE/Chit-PB-MWNTs-HGNs/Au	0.05-75 nM	0.05 nM	[29]
AChE&ChOx/Pt-Au/MWCNT/GCE	0.1-50 nM	0.16 nM	[30]
AChE-CS/Pb-Cu NWs/GCE	15-3000 pM, 1500-9000 nM	4.5 pM	[19]
AChE-MWCNTs-β-CDCHIT/GCE	0.01-10.0 µM	2 nM	[31]
AChE-PAn-PPy-MWCNTs/GCE	0.03-1.5, 3-75 mM	3 nM	[32]
AChE-CS/3DG-CuO NFs/GCE	3 pM-46.665 nM	0.93 pM	[17]
AChE-CS/rGO-TEPA-CuO NWs/GCE	3 pM-60 nM	1.2 pM	This work

Under the optimized conditions, the concentration of malathion was measured by the AChE sensor. DPV response showed that the oxidation peak decreased if the concentration of malathion

increased (Fig. 5A), (a) represented the DPV response of the AChE sensor to ATCl without malathion inhibition, and (b) to (h) were the DPV response of AChE sensor after the inhibition by different concentrations of malathion. $\Delta I = 2.573 \text{Log } C_{mal} + 1.058$ ($R^2 = 0.989$) from 1 ng/mL to 20 μg/mL (3 pM to 60 nM) (Fig. 5B).

Then, the detection limit was about 0.39 ng/mL (1.2 pM) (S/N=3) calculated from the liner curve. As shown in Table 1, the malathion detection range of our biosensor (3 pM-60 nM) was broader and the detection limit was lower compared with previous reports. These results indicated that rGO-TEPA-Cu NWs had excellent conductivity and large specific surface to accelerate electron transfer.

3.5 Interference of AChE sensor

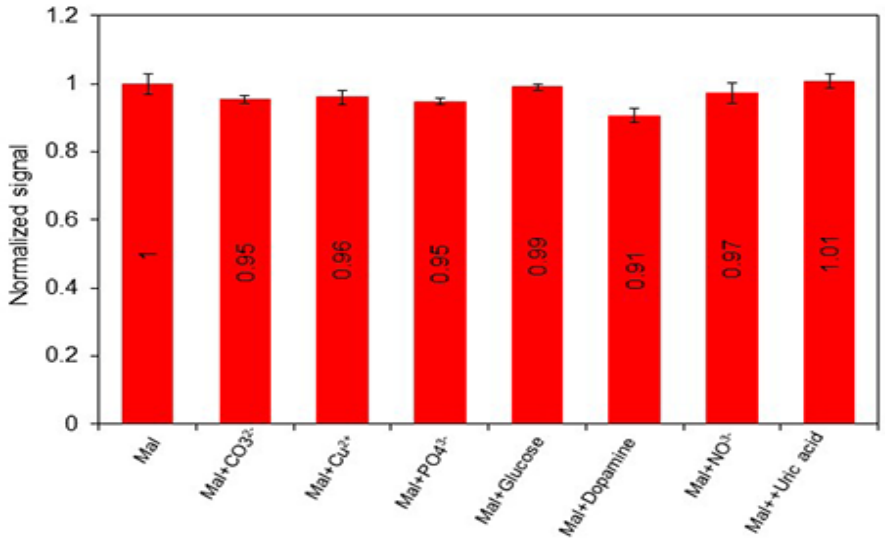

Figure 6. DPV response of AChE-CS/rGO-TEPA-Cu NWs/GCE in 10 ng/mL malathion (mal), 2 mM ATCl and 1 mM CO_3^{2-}, 1 mM Cu^{2+}, 1 mM PO_4^{3-}, 1 mM glucose, 1 mM dopamine, 1 mM NO^{3-}, 1 mM uric acid. n=3.

To assess the ability of AChE-CS/rGO-TEPA-Cu NWs/GCE to resist interfering substances, we performed anti-interference analysis of the sensor. It was reported that some inorganic salt and metal ion could cause interference to nano-based biosensor [33]. We added 1 mM CO_3^{2-}, Cu^{2+}, PO_4^{-3}, Glu, dopamine, NO_3^-, and uric acid to the detection system, and found that the DPV current response did not change much compared with the standard signal. These results suggest that our sensor has good anti-interference ability.

3.6 The stability and reproducibility of AChE biosensor

To assess the reproducibility of our biosensor to detect malathion, we used six different AChE-CS/rGO-TEPA-Cu NWs/GCE electrodes were used. The relative standard deviation (RSD) was 2.3%,

showing good reproducibility. Furthermore, we made six independent DPV measurements and the RSD was 2.6%. These results indicate that the biosensor has acceptable reproducibility.

To assess the stability of our biosensor to detect malathion, we examined current responses of the biosensor for 30 days. After 7 days, the response current decreased to 96.9% of the original signal. After 30 days, the response current decreased to 85.1% of the original signal. These results suggest that the biosensor has acceptable stability.

3.7 Detection of malathion in real samples

To explore practical application of AChE biosensor, actual samples (cabbage and carrots obtained from local market) were tested under the optimal experimental conditions. The recovery values ranged from 95.8% to 101.3%, and the RSD was less than 3.25 (Table 2). These results demonstrated that AChE-CS/rGO-TEPA-Cu NWs/GCE is feasible to detect malathion in real samples.

Table 2. Detection of malathion in real samples by AChE-CS/rGO-TEPA-Cu NWs/GCE biosensor.

Samples	Add (ng/mL^{-1})	Found (ng/mL^{-1})	RSD (%, n=3)	Recovery (%)
Cabbage 1	1	1.21	3.25	97.5
Cabbage 3	50	49.8	2.56	101.3
Cabbage 4	500	500.5	1.35	99.4
Carrots 1	1	0.978	2.89	95.8
Carrots 3	50	51.1	2.21	99.1
Carrots 4	500	499.8	1.28	100.3

4. CONCLUSION

We developed a sensitive and selective AChE-CS/rGO-TEPA-Cu NWs/GCE biosensor for detecting malathion. The biosensor showed high sensitivity and affinity to ATCl. In addition, the biosensor had high sensitivity, reproducibility and stability, and could be applied to detect malathion in vegetable samples.

ACKNOWLEDGMENTS
This study was supported by National Natural Science Foundation of China (No. 31401091), the Guizhou Province "Thousand" Innovative Talents (2015). We gratefully acknowledge the technical assistance of Dr.Guangchao Zang and Dr.Yuchan Zhang. We also thanks to Dr.Yinqun Wang for editing the article language.

References

1. D. E. Lorke and G. A. Petroianu, *J. Appl. Toxicol*., 39 (2019) 101.

2. H. Fan, J. Smuts, P. Walsh, D. Harrison and K. A. Schug, *J. Chromatogr*., 1389 (2015) 120.
3. C. K. Zacharis, C. Christophoridis and K. Fytianos, *J. Sep. Sci.*, 35 (2012) 2422.
4. P. Carullo, M. Chino, G. P. Cetrangolo, S. Terreri, A. Lombardi, G. Manco, A. Cimmino and F. Febbraio, *Sens. Actuators. B. Chem.*, 255 (2018) 3257.
5. Y. Li, Q. Luo, R. Hu, Z. Chen and P. Qiu, *Chinese. Chem. Lett*., 29 (2018) 1845.
6. P. Kumar, K. H. Kim and A. Deep, *Biosens. Bioelectron.*, 70 (2015) 469.
7. Y. Zhang, H. B. Fa, B. He, C. J. Hou, D. Q. Huo, T. C. Xia and Y. Wei, *J. Solid. State. Electr.*, 21 (2017) 1.
8. L. Yang, G. Wang, Y. Liu and M. Wang, *Talanta*, 113 (2013) 135.
9. H. Zhao, X. Ji, B. Wang, N. Wang, X. Li, R. Ni and J. Ren, *Biosens. Bioelectron.*, 65 (2015) 23.
10. L. He, B. Cui, J. Liu, Y. Song, M. Wang, D. Peng and Z. Zhang, *Sens. Actuators. B. Chem.*, 258 (2018) 813.
11. M. R. Willner and P. J. Vikesland, *J. Nanobiotechnol*., 16 (2018) 95.
12. M. Pohanka, *Int. J. Electrochem. Sci.*, 11 (2016) 7440.
13. A. T. Lawal, *Biosens. Bioelectron.*, 141 (2019) 111384.
14. M. Adeel, M. Bilal, T. Rasheed, A. Sharma and H. Iqbal, *Int. J. Biol. Macromol.*, 120 (2018) 1430.
15. O. Moradi, V. K. Gupta, S. Agarwal, I. Tyagi, M. Asif, A. S. H. Makhlouf, H. Sadegh and R. Shahryari-ghoshekandi, *J. Ind. Eng. Chem*., 28 (2015) 294.
16. L. Cao, F. Cheng, R. Zeng, X. Zhao, F. Zhao, Y. Jiang and Z. Chen, *Sens. Actuators. B. Chem.*, 252 (2017) 44.
17. J. Bao, T. Huang, Z. Wang, H. Yang, X. Geng, G. Xu, M. Samalo, M. Sakinati, D. Huo and C. Hou, *Sens. Actuators. B. Chem.*, 279 (2019) 95.
18. D. Huo, Q. Li, Y. Zhang, C. Hou and L. Yu, *Sens. Actuators. B. Chem.*, 199 (2014) 410.
19. D. Song, Y. Li, X. Lu, M. Sun, H. Liu, G. Yu and F. Gao, *Anal. Chim. Acta.*, 982 (2017) 168.
20. L. Zhou, X. Zhang, L. Ma, J. Gao and Y. Jiang, *Biochem. Eng. J.*, 128 (2017) 243.
21. Y. Zhang, L. Su, D. Manuzzi, M. H. de Los, W. Jia, D. Huo, C. Hou and Y. Lei, *Biosens. Bioelectron.*, 31 (2012) 426.
22. P. Lin, S. Lin, P. C. Wang and R. Sridhar, *Biotechnol. Adv.*, 32 (2014) 711.
23. S. Choi, C. Kim, J. M. Suh and H. W. Jang, *Carbon. Energy.*, 1 (2019) 85.
24. Du D, W. Chen, W. Zhang, D. Liu, H. Li and Y. Lin, *Biosens. Bioelectron.*, 25 (2010) 1370.
25. S. P. Adhikari, G. P. Awasthi, K. S. Kim, C. H. Park and C. S. Kim, *Dalton. Trans.,* 32(2018) 4455.
26. S. Liao, Y. Qiao, W. Han, Z. Xie, Z. Wu, G. Shen and R. Yu, *Anal. Chem*., 84 (2012) 45.
27. Š. Štěpánková and K. Vorčáková, *J. Enzym. Inhib. Med. Chem.*, 31 (2016) 180.
28. M. N. Noorhashimah, A. Khairunisak and Z. Lockman, *Solid. State. Phenom.*, 290 (2019) 193.
29. C. Zhang, C. Lei, C. Cen, S. Tang, M. Deng, Y. Li and Y. Du, *Electrochim. Acta.*, 260 (2018) 814.
30. C. Zhai, X. Sun, W. Zhao, Z. Gong and X. Wang, *Biosens. Bioelectron.*, 42 (2013) 124.
31. S. S. Miao, M. S. Wu, L. Y. Ma, X. J. He and H. Yang, *Talanta*, 158 (2016) 142.
32. D. Du, M. Wang, J. Cai and A. Zhang, *Sens. Actuators. B. Chem.*, 146 (2010) 337.
33. S. Krishnan, E. Singh, P. Singh, M. Meyyappan and H. S. Nalwa, *Rsc. Adv.*, 9 (2019) 8778.